CHEMISTRY
A European Journal

A Journal of
ChemPubSoc Europe

Accepted Article

Title: Targeted Delivery of Mannose-Conjugated BODIPY Photosensitizer by Nanomicelles for Photodynamic Breast Cancer Therapy

Authors: Jian Yin, Quan Zhang, Ying Cai, Qiu-Yan Li, Lin-Na Hao, Zheng Ma, and Xiao-Jun Wang

This manuscript has been accepted after peer review and appears as an Accepted Article online prior to editing, proofing, and formal publication of the final Version of Record (VoR). This work is currently citable by using the Digital Object Identifier (DOI) given below. The VoR will be published online in Early View as soon as possible and may be different to this Accepted Article as a result of editing. Readers should obtain the VoR from the journal website shown below when it is published to ensure accuracy of information. The authors are responsible for the content of this Accepted Article.

To be cited as: *Chem. Eur. J.* 10.1002/chem.201702935

Link to VoR: http://dx.doi.org/10.1002/chem.201702935

Supported by
ACES

WILEY-VCH

Targeted Delivery of Mannose-Conjugated BODIPY Photosensitizer by Nanomicelles for Photodynamic Breast Cancer Therapy

Quan Zhang,[a] Ying Cai,[a] Qiu-Yan Li,[b] Lin-Na Hao,[a] Zheng Ma,[b] Xiao-Jun Wang,*[b] and Jian Yin*[a]

Abstract: The targeted delivery of a photosensitizer (PS) with appropriate carriers represents an attractive means of selectively delivering cargo to target tissues or subcellular compartments for photodynamic therapy (PDT). Herein, we report a three-arm distyryl BODIPY derivative conjugated with mannose units (denoted by BTM) that can co-assemble with Tween 80 to form nanomicelles (BTM-NMs) for targeted PDT. MDA-MB-231 breast cancer cells recognized and specifically internalized BTM-NMs via mannose receptor-mediated endocytosis with preferential accumulation in the lysosomes. These NMs could disassemble in cell lysosomes and subsequently induce highly efficient singlet oxygen ($^1O_2$) generation upon light irradiation. $^1O_2$ disrupted the lysosomal membrane and promoted the escape of BTM from the lysosome into the cytoplasm, thereby resulting in the efficient and selective killing of cancer cells through PDT. This study may provide a new strategy for designing targeted PDT systems to fight cancer.

Introduction

Photodynamic therapy (PDT), a minimally invasive treatment of tumours and other diseases, has attracted an increasing amount of attention.[1] The PDT process comprises three key elements: light, oxygen, and a photosensitizer (PS). Cancer treatment via PDT involves the uptake of a PS by tumour tissue and irradiation with light of the appropriate wavelength. Upon irradiation, the excited PS transfers energy to surrounding molecular oxygen, resulting in generation of highly cytotoxic reactive oxygen species (ROS), primarily singlet oxygen ($^1O_2$).[2] To date, an extensive series of PSs have been developed, including porphyrins,[3] chlorins,[4] phthalocyanines,[5] and boron dipyrromethene (BODIPY).[6] However, most PSs are hydrophobic organic molecules and cannot target malignant tissues,[7] which considerably hampers their practical applications for PDT.

To overcome the solubility and target specificity limitations of PSs, many nanocarriers, including liposomes,[8] polymeric nanoparticles,[9] nanomicelles (NMs),[10] and inorganic nanoparticles,[11] have been developed to deliver PSs for cancer PDT. Compared with free PSs, PS-loaded nanocarriers have obvious advantages, including improving bioavailability, prolonging the blood circulation time, and facilitating the passive targeting and accumulation of the PS at the tumour sites via the enhanced permeability and retention (EPR) effect.[12] Moreover, grafting targeting units, such as antibodies and folic acid, onto the nanocarrier surface allows active targeting, thus reducing the side effects by decreasing the interactions of nanocarriers with healthy cells.[13]

Conjugating hydrophobic PSs with carbohydrates can make them amphiphilic, thereby improving their solubility in physiological fluids and promoting cellular recognition via specific carbohydrate-protein interactions on cell surfaces.[14] For example, a significant increase in the in vitro photosensitizing efficiency of porphyrins conjugated with mannose compared to that of their unconjugated analogue has been reported.[15] The mannose receptor (MR) is overexpressed on the surfaces of some malignant cells,[16] and mannose-functionalized nanocarriers can be internalized into cancer cells via receptor-mediated endocytosis.[17] Although the individual binding of mannose with the MR is weak, this interaction can be improved by incorporating multiple mannose ligands onto one nanocarrier, a process that increases the binding intensity and specificity between the mannose-functionalized nanocarriers and overexpressed MRs on cancer cells.[18] To the best of our knowledge, no study has been reported on the use of carbohydrate-conjugated PS to construct nanocarriers, and thus to make them applicable in targeted PDT.

In this work, we reported a new delivery system for a mannose-conjugated BODIPY PS (Scheme 1). A three-arm distyryl BODIPY PS conjugated with mannose units was synthesized (denoted by BTM) and co-assembled with Tween 80 to form BTM-loaded nanomicelles (denoted by BTM-NMs). The molecular design of BTM is based on the following factors: (1) 2,6-Halogenation (I) of the BODIPY core renders it an efficient PS for ROS generation because of the heavy atom effect; (2) Incorporating distyryl moieties into the BODIPY core is expected to shift the absorption to the long wavelength region with a maximum of 665 nm, which enables deep-tissue penetration; (3) Because of its inherent amphiphilicity, BTM can co-assemble with Tween 80 to generate stable and well-defined NMs in aqueous media; and (4) NMs can provide a platform for the multivalent presentation of mannose, which increases their selectivity for MDA-MB-231 breast cancer cells with overexpressed MRs. Targeted PDT with the BTM-NMs was demonstrated through their phototoxicity to MDA-MB-231 cancer cells and nontoxicity to MCF-10A normal cells.

[a] Prof. Q. Zhang, Y. Cai, L.-N. Hao, Prof. J. Yin
Key Laboratory of Carbohydrate Chemistry and Biotechnology
Ministry of Education, School of Biotechnology
Jiangnan University, Wuxi, 214122 (P. R. China)
E-mail: jianyin@jiangnan.edu.cn

[b] Dr. Q.-Y. Li, Z. Ma, Prof. X.-J. Wang
Jiangsu Key Laboratory of Green Synthetic Chemistry for Functional Materials, School of Chemistry and Materials Science
Jiangsu Normal University, Xuzhou, 221116, (P. R. China)
E-mail: xjwang@jsnu.edu.cn

Supporting information for this article is given via a link at the end of the document.

Accepted Manuscript

This article is protected by copyright. All rights reserved.

Results and Discussion

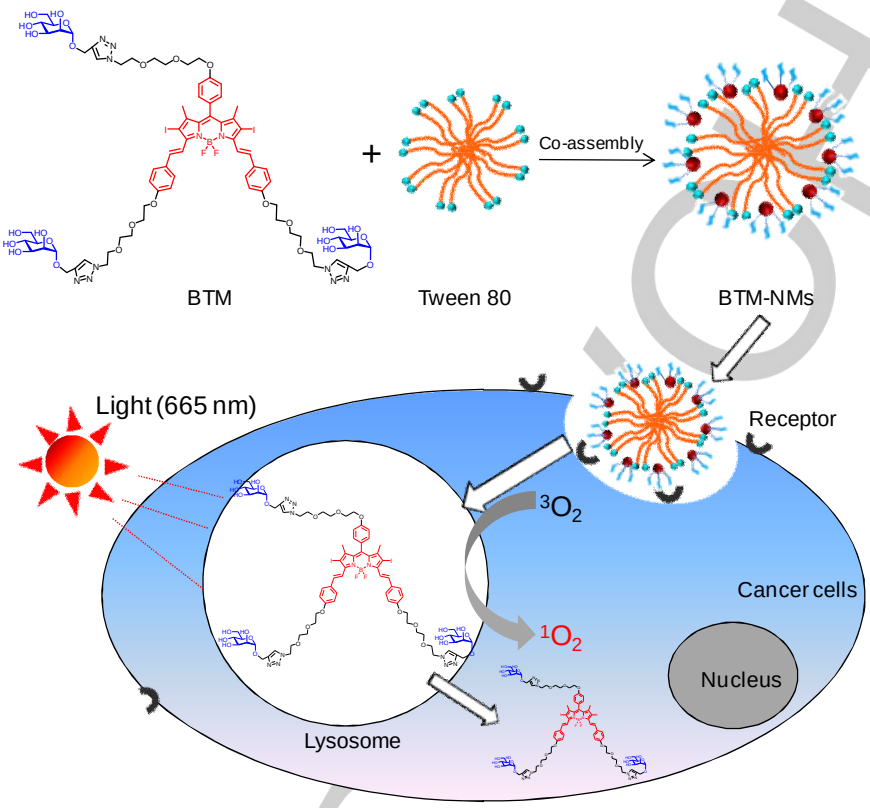

Scheme 1. Schematic illustration of the preparation of BTM-NMs and their application in targeted PDT.

The synthesis of BTM is shown in Scheme 2. First, compound **1** was prepared according to reported procedures,[19] and the experimental details are provided in the Supporting Information (Scheme S1). Compound **1** was reacted with 2,4-dimethylpyrrole in the presence of trifluoroacetic acid, and then 2,3-dichloro-5,6-dicyano-1,4-benzoquinone (DDQ) and $BF_3{\cdot}Et_2O$ were added to afford **2**, which was further transformed via reaction with 1-iodo-2,5-pyrrolidinedione (NIS) into **3**. Compound **4** was obtained in 59% yield by reacting **3** with **1** in the presence of piperidine. Mannose was conjugated to **4** via the copper-catalysed click reaction between **4** and **5**, and BTM was obtained in 41% yield after high-performance liquid chromatography (HPLC) purification. The chemical structures of the intermediate products and BTM were characterized using NMR and MS (Figure S1−S8, Supporting Information). To verify the molecular weight and purity of BTM, HPLC analysis was performed, and the results are shown in Figure 1. The HPLC profile showing one retention time of BTM at 10.05 min indicates the high purity of the compound. The MS data show that the molecular weight of BTM (*m/z*, $M+Na^+$) is 1949.31, which is consistent with the calculated value (*m/z*, $M+Na^+$, 1949.30). These experimental results confirm that BTM has been synthesized successfully.

BTM was also characterized by FT-IR spectroscopy and UV-Vis spectrophotometry. In the FT-IR spectrum of compound **4**, the absorption band at 2100 cm^{-1} is attributed to the stretching vibration of the azide groups (Figure S9, Supporting Information). After the click reaction between compounds **4** and **5**, the spectrum of BTM shows no absorption band at 2100 cm^{-1}. The strong stretching absorption band appearing at 1660 cm^{-1} appears due to the formation of the triazole linkage. In the UV-Vis spectrum, BTM has a maximum absorption at 665 nm that strictly followed the Lambert-Beer law, indicating that BTM did not form aggregates in dimethylformamide (DMF) (Figure S10, Supporting Information).

Accepted Manuscript

This article is protected by copyright. All rights reserved.

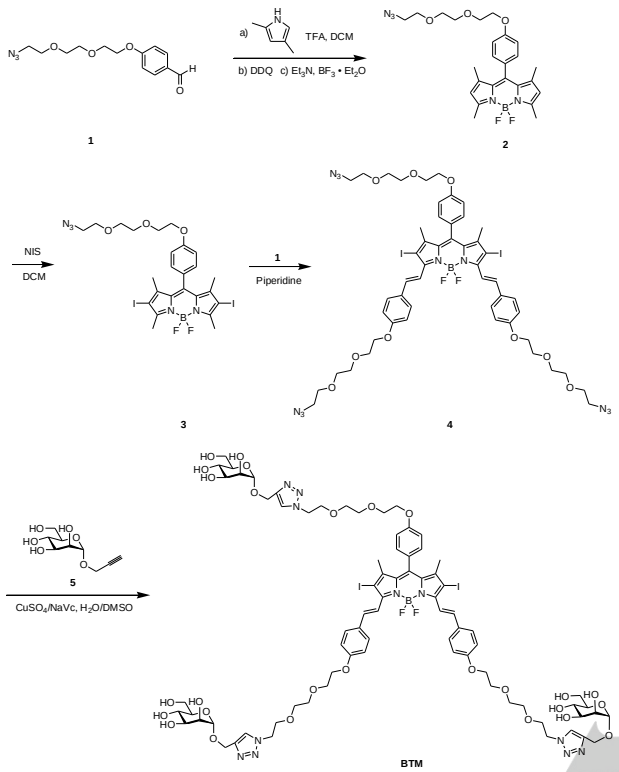

Scheme 2. Synthesis of BTM.

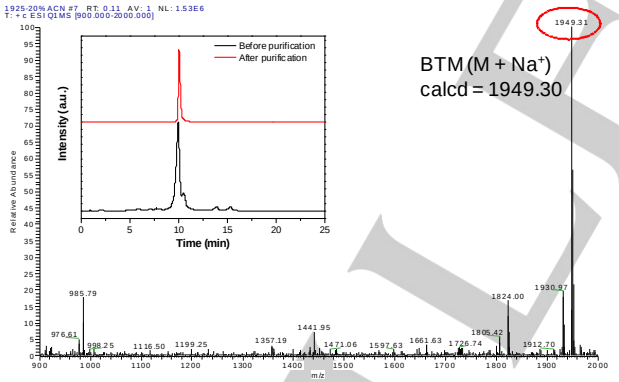

Figure 1. Mass spectrum of BTM. Inset: The HPLC profiles of BTM before and after purification.

After successfully synthesizing BTM, we proceeded to prepare the BTM-NMs using a reprecipitation technique, i.e., slowly adding a DMF solution of BTM into deionized water containing 0.1 vol% Tween 80. To investigate the aggregation process, we measured the fluorescence spectra of BTM aggregates formed in the DMF/water mixture by varying the fraction of water (f_w). In pure DMF, BTM showed strong fluorescence emission at 678 nm (Figure S11, Supporting Information) with a fluorescence quantum yield (Φ) of 0.17 relative to zinc(II) phthalocyanine (ZnPc) (0.28).[20] When the water content in DMF was increased, an obvious decrease in the fluorescence intensity of BTM was observed (Figure 2a). When the f_w in DMF was 70%, BTM clearly formed well-dispersed nanoaggregates and exhibited a fluorescent decrease at 678 nm (Figure 2b). After DMF was removed by dialysis, a stable NM solution with a concentration of 0.4 mg mL^{-1} was obtained, and the BTM content in the BTM-NMs was estimated as 39 wt%.

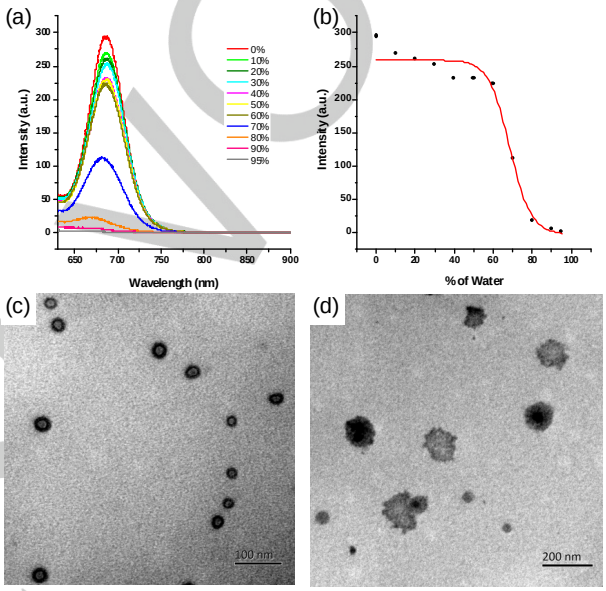

Figure 2. (a) Fluorescence spectra (excitation at 610 nm) of BTM recorded in DMF solutions with increasing water content. The coloured lines indicate the volume percentage of water during the measurements. (b) Corresponding plots of emission intensity changes for BTM versus water content. (c) TEM image of as-prepared BTM-NMs when the f_w in DMF was 70%. (d) TEM image of larger nanoaggregates when the f_w in DMF was 80%.

The morphology of the resulting BTM-NMs was determined using transmission electron microscopy (TEM). According to TEM, the BTM-NMs were roughly spherical in shape (Figure 2c) and were approximately 29.0 ± 3.3 nm in size. Notably, larger nanoaggregates with a wide size distribution (~10 nm to 200 nm) were obtained when the f_w in DMF was 80% during the nanoaggregate preparation process (Figure 2d). In addition, irregular nanoaggregates were obtained when a 30% BTM solution in DMF was mixed with 70% water without 0.1 vol% Tween 80 (Figure S12, Supporting Information). These results confirm that BTM could co-assemble with Tween 80 to generate BTM-NMs when the f_w in DMF was 70%. Dynamic light scattering (DLS) analysis showed that the average hydrodynamic diameter of the BTM-NMs in water was approximately 56.8 ± 4.4 nm (PDI, 0.298) (Figure S13, Supporting Information). The physiological stability of the BTM-NMs was evaluated by suspending them in culture medium containing 10% serum. No significant size change was observed

Accepted Manuscript

This article is protected by copyright. All rights reserved.

after incubating the BTM-NMs in this medium for at least 72 h, indicating that the BTM-NMs have good stability under physiological conditions (Figure S14, Supporting Information).

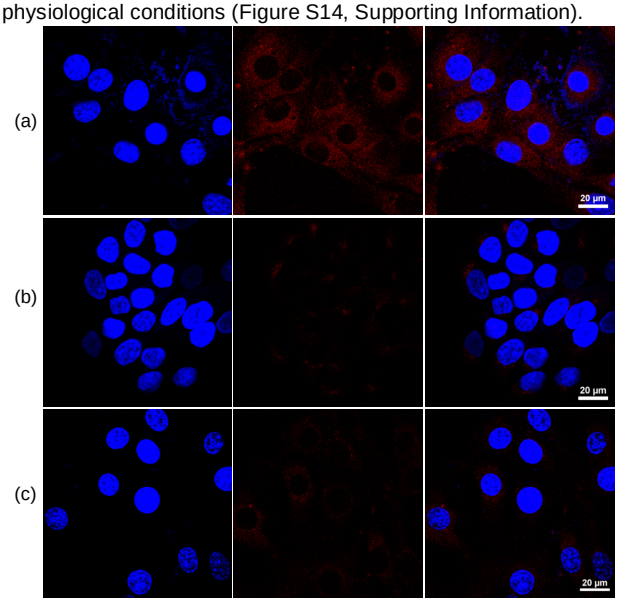

Figure 3. CLSM images of (a) MDA-MB-231 cancer cells and (b) MCF-10A cells treated with BTM-NMs (at a BTM dose of 8 μg mL^{-1}) for 24 h. CLSM images of (c) MDA-MB-231 cancer cells treated with BTM-NMs (at a BTM dose of 8 μg mL^{-1}) with mannose (1 mM) competition. For each panel, the three images from left to right show cell nuclei stained by DAPI (blue), BTM molecules in cells (red), and overlays of the two sets of images, respectively.

The cellular uptake behaviour of BTM-NMs was monitored using confocal laser scanning microscopy (CLSM), as shown in Figure 3. MDA-MB-231 breast cancer cells with high MR expression (MR+) were chosen as a positive control,[14b,16b] and normal MCF-10A cells with low MR expression (MR-) were used as a negative control. Both MDA-MB-231 and MCF-10A cells were treated with BTM-NMs for 24 h. After the cells were washed with a phosphate buffered saline (PBS, pH 7.4) solution, the cell nuclei were stained with 4',6-diamidino-2-phenylindole (DAPI) before observation. The blue fluorescence from DAPI signifies the cell nucleus, and the red fluorescence arises from the BTM molecules. More red fluorescent spots were observed inside MDA-MB-231 cancer cells than in MCF-10A cells, in which a very weak fluorescence was observed. These results indicated a much higher uptake of the BTM-NMs by the MDA-MB-231 cancer cells (Figure 3a) than by the MCF-10A cells (Figure 3b), which was due to the low level of MR expression on the cellular membranes of the latter cell line. To confirm the association between BTM-NM uptake and MR expression, competition inhibition studies were performed using free mannose to compete with the BTM-NMs for binding with MR on the surface of cancer cells, potentially reducing the uptake of BTM-NMs into MDA-MB-231 cells. As shown in Figure 3c, when MDA-MB-231 cells were incubated with both BTM-NMs and free mannose under the same conditions, a significant inhibition of BTM-NM uptake due to MR competition was observed. These observations were further confirmed using ImageJ software analysis, which showed a statistically significant decrease in the red fluorescent intensity in BTM-NM–treated MDA-MB-231 cells after adding free mannose (Figure S15, Supporting Information). These results suggest that the BTM-NMs were taken up significantly more in the absence of mannose than in the presence of mannose because of MR-mediated endocytosis. Thus, BTM-NMs not only selectively target cancer cells but also improve the internalization of PSs within targeted cancer cells.

The $^1O_2$ generation efficiency was studied in DMF by measuring the absorbance decrease of 1,3-diphenylisobenzofuran (DPBF) upon 665-nm LED light irradiation (Figure S16, Supporting Information). The $^1O_2$ quantum yield (Φ_Δ) of BTM was determined to be 0.58 using ZnPc as the standard PS (Φ_Δ = 0.60 in DMF).[21] Moreover, the $^1O_2$ generation capability of BTM-NMs was evaluated using a chemical method with 9,10-anthracenediylbis(methylene)dimalonic acid (ABDA) as the $^1O_2$ trapping agent.[22] ABDA reacts with $^1O_2$ to produce the corresponding endoperoxide and then change its absorption. A typical absorption spectrum of ABDA in water shows two characteristic bands at 412 and 435 nm, and no significant change was observed when an aqueous solution of ABDA was irradiated with a 665-nm LED light (20 mW cm^{-2}, 10 min) (Figure S17, Supporting Information). However, the absorption of ABDA decreased continuously when a mixture of ABDA and BTM-NMs in water was irradiated under the same conditions. Thus, these results confirmed the efficient generation of $^1O_2$ from BTM-NMs in aqueous conditions.

The intracellular $^1O_2$ production of the BTM-NMs was investigated using fluorescence microscopy imaging with the probe dichlorofluorescein diacetate (DCFH-DA), which can be oxidized by $^1O_2$ into dichlorofluorescein (DCF), a compound that emits green fluorescence.[23] MDA-MB-231 cancer cells were incubated with BTM-NMs for 24 h, and then DCFH-DA was added, followed by irradiation with the 665-nm LED light (20 mW cm^{-2}) for 10 min. After being washed with PBS, the cells were monitored in real time via excitation at 488 nm using a confocal microscope. As shown in Figure 4a, obvious DCF fluorescence can be detected after 665-nm light irradiation, whereas no fluorescence was observed without irradiation. In addition, the morphology of the MDA-MB-231 cancer cells significantly changed after irradiation, indicating that the BTM-NPs can induce serious photodynamic cellular damage and eventual apoptosis. Moreover, the fluorescence intensity clearly decreased in the presence of sodium azide, a well-known $^1O_2$ scavenger (Figure 4b).[24] These results indicate that BTM can efficiently produce intracellular $^1O_2$ in the irradiated region after the internalization of BTM-NMs in MDA-MB-231 cancer cells via receptor-mediated endocytosis. Based on our cell experiment results, $^1O_2$ was produced from endocytosed BTM-NMs in the cells (Figure 3), and the red fluorescence of BTM was observed inside the cell (Figure 3). Thus, we can conclude that BTM-NMs disassemble into BTM molecules in the MDA-MB-231 cancer cells after being internalized via receptor-mediated endocytosis.

Accepted Manuscript

This article is protected by copyright. All rights reserved.

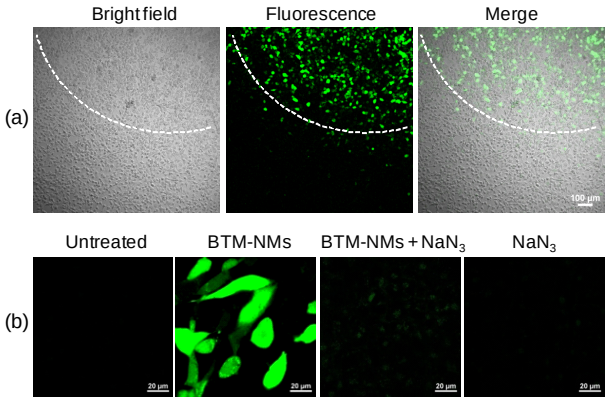

Figure 4. (a) CLSM images of MDA-MB-231 cancer cells treated with BTM-NMs (at a BTM dose of 8 μg mL^{-1}) for 24 h followed by DCFH-DA staining and irradiation (665 nm, 20 mW cm^{-2}) for 15 min. (b) Detection of intracellular $^1O_2$ by DCFH-DA staining in MDA-MB-231 cancer cells incubated with BTM-NMs (at a BTM dose of 8 μg mL^{-1}) in the presence or absence of sodium azide. The green fluorescence is from the product of DCFA-DA oxidation by $^1O_2$.

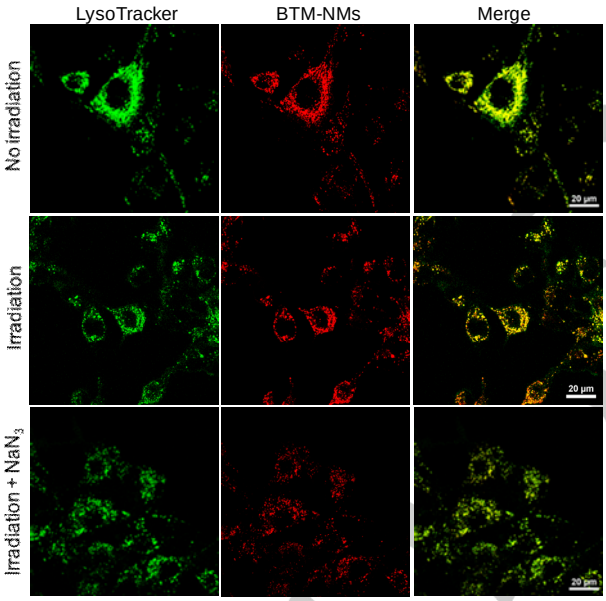

Figure 5. CLSM images of live MDA-MB-231 cells after 24 h of incubation with BTM-NMs (at a BTM dose of 8 μg mL^{-1}) with or without irradiation. When colocalized, the green and red spots produce a yellow colour, which is due to BTM molecules trapped inside the cell lysosomes.

To investigate the intracellular distribution of the BTM-NMs, MDA-MB-231 breast cancer cells were incubated with the nanocarriers for 24 h and then treated with LysoTracker, a marker of late endosomal and lysosomal vesicles. CLSM was employed to observe the BTM-NM intracellular distribution with and without irradiation. Green fluorescence denotes the LysoTracker-labelled lysosomes, and red fluorescence is from the intracellular BTM molecules. The NMs located inside the lysosomes were yellow because of the overlap between the green (LysoTracker) and red (BTM) fluorescent spots. Figure 5 shows that the red BTM fluorescence had a colocalization percentage of approximately 91% with the lysosomes in the absence of irradiation, indicating effective endocytosis into the lysosomes upon cell internalization. However, BTM exhibited a poor colocalization of 45% with the lysosomes in the presence of irradiation, suggesting that BTM could escape from the lysosome after irradiation and was distributed in the cytoplasm. Interestingly, the lysosomal disruption was significantly inhibited in the presence of sodium azide under irradiation, as under these conditions a colocalization percentage between BTM and lysosomes of 82% was observed. These results reveal that lysosomal disruption is attributable to the damage caused by the intracellular $^1O_2$ generated upon irradiation.

To observe the effects of targeted PDT, a glucose-conjugated BODIPY PS (BTG) was synthesized using similar methods to BTM, except glucose units were used instead of mannose units. Subsequently, glucose-functionalized nanomicelles (BTG-NMs) were prepared as a control sample. MDA-MB-231 cancer cells were incubated with BTM-NMs or BTG-NMs at the same PS-equivalent dose (8 μg mL^{-1}). After 24 h, the cells were stained with DAPI to examine changes in the nuclear morphology after PDT.[25] As shown in Figure 6a, the nuclei in MDA-MB-231 cells treated with BTG-NMs and irradiated with 665 nm LED light irradiation (20 mW cm^{-2}) did not change. By contrast, the nuclei of MDA-MB-231 cancer cells treated with BTM-NMs under the same irradiation conditions were significantly damaged. In addition, BTG-NMs and BTM-NMs were individually incubated with MDA-MB-231 cancer cells under the same conditions for 24 h. After being washed three times with PBS, the cells were irradiated with 665 nm LED light (20 mW cm^{-2}) for 30 min and then co-stained with calcein-AM and PI.[26] Green fluorescence represents live cells stained with calcein-AM, and red fluorescence denotes dead cells stained with PI. After being washed another three times with PBS, the cells were monitored using a confocal microscope. As shown in Figure 6b, only a few cells incubated with BTG-NMs were photodamaged, whereas almost no live cells were found after they were treated with BTM-NMs. These results confirmed that the BTM-NMs have greater cellular uptake and intracellular ROS production than the BTG-NMs. Moreover, we can clearly observe that barely any cells in the irradiation region are alive, which further demonstrates that BTM-NMs can specifically kill cancer cells under 665-nm light irradiation (Figure S18, Supporting Information).

Accepted Manuscript

This article is protected by copyright. All rights reserved.

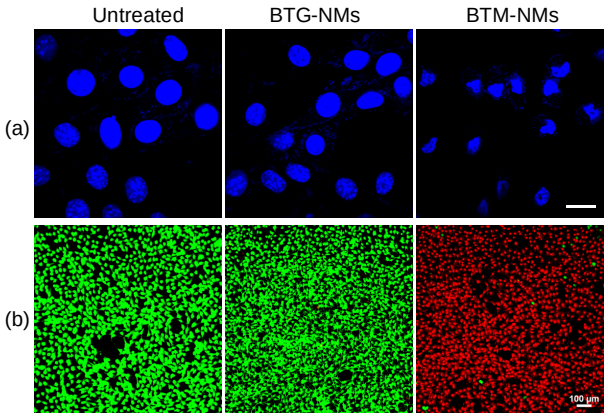

Figure 6. (a) CLSM images of cell nuclei stained by DAPI for assessing nuclear damage after light irradiation (665 nm, 20 mW cm^{-2}) for 30 min. Scale bar: 20 μm. (b) CLSM images of a live/dead assay (calcein-AM/PI) performed on co-stained MDA-MB-231 cells after being incubated with BTG-NMs or BTM-NMs and then being irradiated (665 nm, 20 mW cm^{-2}) for 30 min. The cells were co-stained with calcein-AM (green, live cells) and PI (red, dead cells). Scale bar: 100 μm.

The targeted PDT efficacy of the BTM-NMs was further evaluated using the 3-(4,5-dimethylthiazol-2-yl)-2,5-diphenyltetrazolium bromide (MTT) assay.[27] First, MDA-MB-231 (MR+) and MCF-10A (MR-) cells were incubated with different concentrations of either BTG-NMs or BTM-NMs. After being washed with PBS, the cells were irradiated with the 665-nm LED light for 30 min. For the MCF-10A cells, the two samples showed similar cell viability (Figure 7a). Conversely, MDA-MB-231 cells treated with the BTM-NMs exhibited much lower cell viability than those treated with the BTG-NMs (Figure 7b), indicating that the targeting effect of BTM-NMs through MR-mediated endocytosis increased the internalization of the NMs and thus led to a high percentage of BTM being taken up by MDA-MB-231 cells. Next, we assessed the phototoxicity of BTG-NMs and BTM-NMs with different light irradiation times. Whereas the phototoxicity of the BTM-NMs was found to be similar to that of the BTG-NMs for MCF-10A normal cells (Figure 7c), a significant difference between the two NMs was observed for MDA-MB-231 cancer cells. As the irradiation time was prolonged, the phototoxicity of the BTM-NMs gradually became higher than that of the BTG-NMs (Figure 7d). These results confirm the time-dependent PDT effect and MR-mediated cancer cell targeting properties of the BTM-NMs. Furthermore, the dark toxicity of the BTG-NMs and BTM-NMs was also investigated (Figure S19, Supporting Information). Without light irradiation, a negligible toxicity to both MDA-MB-231 cells and MCF-10A cells was observed for the two NMs, even at a high concentration (30 μg mL^{-1}). No concentration-dependent toxic effect was found, indicating that the internalization of the present dose of NMs is minimally cytotoxic.

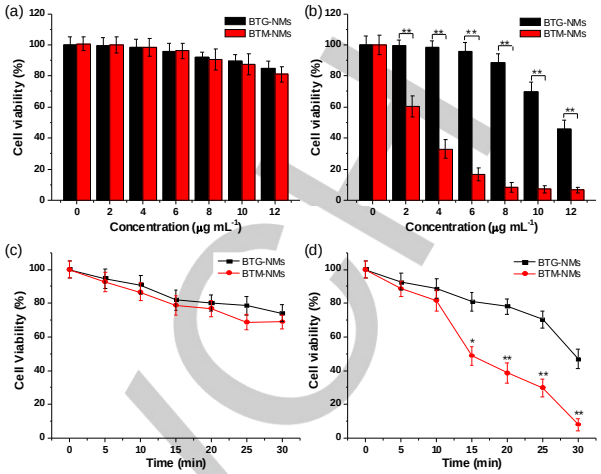

Figure 7. Viability of (a) MCF-10A normal cells and (b) MDA-MB-231 cancer cells after being incubated for 24 h with different PS concentrations of BTG-NMs or BTM-NMs and then being irradiated (665 nm, 20 mW cm^{-2}) for 30 min. Time-dependent PDT effects on (c) MCF-10A normal cells and (d) MDA-MB-231 cancer cells incubated with BTG-NMs or BTM-NMs at the same PS-equivalent dose of 12 μg mL^{-1} and then irradiated (665 nm, 20 mW cm^{-2}) for different times.

Conclusions

In summary, a three-arm distyryl BODIPY PS conjugated with mannose units was synthesized and used to prepare mannose-functionalized nanomicelles for targeted PDT against MDA-MB-231 breast cancer cells. After selectively being internalized into MDA-MB-231 breast cancer cells via receptor-mediated endocytosis, the BTM-NMs can disassemble into BTM molecules in the cell lysosomes and efficiently generate $^1O_2$ upon light irradiation. $^1O_2$ disrupted the lysosomal membrane and promoted the escape of BTM from lysosome into the cytoplasm, thereby facilitating $^1O_2$ reaching organelles such as the nucleus and mitochondria for enhanced photodynamic cell damage. The BTM-NMs exhibit excellent targeted delivery of the PS that not only leads to selective cancer cell death but also minimizes damage to normal cells after irradiation. Therefore, the current research has demonstrated the potential of this system to deliver PSs for enhanced PDT of breast cancer cells.

Experimental Section

Materials

2-[2-(2-chloroethoxy)ethoxy]ethanol, ABDA, boron trifluoride diethyl etherate ($BF_3{\cdot}Et_2O$), copper sulfate pentahydrate ($CuSO_4{\cdot}5H_2O$), DAPI, 2,3-dichloro-5,6-dicyano-1,4-benzoquinone (DDQ), DCFH-DA, dichloromethane (DCM, 99.5%), 2,4-dimethylpyrrole, 4-(dimethylamino)pyridine (DMAP), DMF (99.5%), DPBF, MTT, Dulbecco's modified Eagle's medium (DMEM), ethyl acetate (EtOAc, 99.5%), foetal bovine serum (FBS), 4-hydroxybenzaldehyde, NIS, LysoTracker probes (Green DND), α-D-mannose, methanol (MeOH, 99.5%), PBS (pH 7.4),

Accepted Manuscript

This article is protected by copyright. All rights reserved.

piperidine, sodium ascorbate, tetrahydrofuran (THF, 99.0%), *p*-toluenesulfonic acid (TsOH), *p*-toluenesulfonyl chloride (TsCl), triethylamine (Et_3N), trifluoroacetic acid (TFA), and trimethylsilyl trifluoromethanesulfonate (TMSOTf) were purchased commercially and used without further purification. All aqueous solutions were prepared using ultrapure water from a Milli-Q system (Millipore, USA).

Characterization

^{1}H NMR spectra were obtained on a Bruker Avance spectrometer operating at 400 MHz. HPLC was performed on an Agilent HPLC system equipped with a UV detector (665 nm). The analytical column was an Agilent Zorbax XDB-C18 (5 μm particles, 4.6 × 150 mm). The following two eluents were used: A contained 100% H_2O, and B contained 100% CH_3OH. B was increased from 70% to 100% over 20 min at a flow rate of 0.8 mL min^{-1}. TEM images were obtained on a HITACHI H-7650 TEM at 80 kV. UV-Vis absorption spectra and fluorescence spectra were recorded on a Hitachi U-3900 UV-Vis spectrophotometer and a Hitachi F-7000 spectrophotometer, respectively. Hydrodynamic diameter and zeta potential measurements were performed at 25 °C on a Malvern Zetasizer NanoZS instrument. All the measurements were performed with the NMs suspended in filtered water or filtered cell culture medium at a concentration of 30 μg mL^{-1}. A Nikon confocal microscope was used for cell imaging. An LED lamp with a light density of 20 mW cm^{-2}, which was monitored using a light power meter (NEWPORT Model 842-PE), was used.

Synthesis of compound 1

The synthetic procedures are described in the Supporting Information.

Synthesis of compound 2

To a solution of compound **1** (1.1 g, 3.94 mmol) in anhydrous DCM (120 mL) were added 2,4-dimethylpyrrole (0.9 g, 9.46 mmol) and TFA (0.3 mL) at room temperature. The mixture was stirred under a nitrogen atmosphere for 12 h. To this solution was added DDQ (2.0 g, 8.16 mmol), and the resulting mixture was stirred for 30 min at room temperature. After the mixture was cooled in an ice bath, Et_3N (10 mL, 135.4 mmol) was added dropwise to the mixture. After 30 min, $BF_3{\cdot}Et_2O$ (12 mL, 95.12 mmol) was added dropwise, and the reaction mixture was stirred for 10 h at 0 °C and allowed to warm to room temperature. After the mixture was diluted with DCM (500 mL) and washed with water (400 mL), the organic layer was dried over anhydrous Na_2SO_4. Following evaporation of the solvent, the product was purified by column chromatography on silica gel (DCM/EtOAc=50:1) to provide compound **2** (0.58 g, yield: 30%). ^{1}H NMR (400 MHz, $CDCl_3$) δ=1.42 (s, 6H), 2.54 (s, 6H), 3.40 (t, J=5.0, 2H), 3.71 (m, 4H), 3.77 (m, 2H), 3.92 (dd, J=5.6, 3.8, 2H), 4.19 (dd, J=5.7, 3.8, 2H), 5.97 (s, 2H), 7.02 (d, J=8.6, 2H), 7.15 (d, J=8.6, 2H). ESI-MS: m/z calcd for $C_{25}H_{30}BF_2N_5O_3$: 497.24; found: 519.96 [M+Na]$^+$.

Synthesis of compound 3

To a solution of compound **2** (0.3 g, 0.61 mmol) in DCM (30 mL) was added 1-iodo-2,5-pyrrolidinedione (NIS) (0.33 g, 1.47 mmol) at room temperature, and the resulting mixture was stirred in the dark for 5 h. After the solvent was removed under reduced pressure, the residue was purified by column chromatography on silica gel (DCM/EtOAc=100:1) to afford compound **3** (0.42 g, yield: 92%). ^{1}H NMR (400 MHz, $CDCl_3$) δ=1.44 (s, 6H), 2.64 (s, 6H), 3.41 (t, J=5.0, 2H), 3.71 (m, 4H), 3.80 (m, J=5.3, 2.1, 2H), 3.94 (dd, J=5.6, 3.7, 2H), 4.21 (dd, J=5.7, 3.7, 2H), 7.13 (d, J=8.6, 2H), 7.05 (d, J=8.6, 2H). ^{13}C NMR (101 MHz, $CDCl_3$) δ=159.76, 156.57, 145.35, 141.53, 131.70, 130.17, 129.05, 126.88, 115.50, 70.95, 70.79, 70.14, 69.80, 67.57, 50.70, 29.70, 22.70, 17.18, 15.99, 14.13. ESI-MS: m/z calcd for $C_{25}H_{28}BF_2I_2N_5O_3$: 749.03; found: 771.97 [M+Na]$^+$.

Synthesis of compound 4

To a solution of compound **3** (0.3 g, 0.40 mmol) in toluene (55 mL) were added compound **1** (0.34 g, 1.22 mmol), piperidine (3 mL), and a catalytic amount of TsOH under a nitrogen atmosphere, and then the resulting solution was stirred for 5 h at 140 °C. After being cooled to room temperature, the reaction mixture was diluted with DCM (400 mL) and washed twice with water (600 mL). The organic layer was dried over anhydrous Na_2SO_4, and the solvent was evaporated *in vacuo*. The crude product was purified by column chromatography on silica gel (DCM/EtOAc=25:2) to provide compound **4** (0.30 g, yield: 59%). ^{1}H NMR (400 MHz, $CDCl_3$) δ=1.50 (s, 6H), 3.41 (q, J=5.9, 5.0, 6H), 3.75 (m, 18H), 3.92 (m, 6H), 4.21 (m, 6 H), 6.97 (d, J=8.8, 4H), 7.06 (d, J=8.6, 2H), 7.16 (d, J=8.6, 2H), 7.59 (m, 6H), 8.12 (d, J=16.9, 2H). ^{13}C NMR (101 MHz, $CDCl_3$) δ=158.90, 149.39, 144.70, 137.98, 132.23, 128.77, 128.59, 128.20, 126.46, 115.82, 114.47, 113.98, 69.92, 69.75, 69.10, 68.78, 66.56, 49.70, 28.67, 21.67, 16.69. ESI-MS: m/z calcd for $C_{51}H_{58}BF_2I_2N_{11}O_9$: 1271.26; found: 1294.40 [M+Na]$^+$.

Synthesis of BTM

To a solution of compound **4** (100 mg, 78.67 μmol) in DMF and H_2O (8 mL, 15:1, v/v) were added compound **5** (86 mg, 394.12 μmol), $CuSO_4{\cdot}5H_2O$ (6.5 mg, 26.09 μmol), and sodium ascorbate (8.7 mg, 43.92 μmol) at room temperature. The reaction mixture was stirred at room temperature for 48 h. After the insoluble solid was removed by filtration, the solvent was removed *in vacuo*. The residue was dissolved in H_2O and purified using C18 reversed-phase HPLC. The product was lyophilized to afford **BTM** (62 mg, 41%). ^{1}H NMR (400 MHz, DMSO-d_6) δ=1.47 (s, 6H), 3.36 – 3.63 (m, 30H), 3.66 – 3.79 (m, 10H), 3.84 (m, 5H), 4.15 (m, 6H), 4.46 – 4.59 (m, 14H), 4.67 (dd, *J*=12.2, 2.9, 3H), 4.73 (m, 7H), 7.07 (d, J=7.3, 4H), 7.16 (d, *J*=8.3, 2H), 7.34 (d, *J*=8.3, 2H), 7.44 (d, *J*=5.3, 2H), 7.58 (d, *J*=8.4, 4H), 8.10 (m, 5H). ^{13}C NMR (101 MHz, DMSO-d_6) δ=160.38, 143.86, 139.14, 129.41, 129.09, 124.91, 115.78, 99.46, 70.68, 70.26, 70.03, 69.18, 67.86, 67.48, 61.77, 58.51, 56.96, 49.81, 17.77. ESI-MS: m/z calcd for $C_{78}H_{100}BF_2I_2N_{11}O_{27}$: 1926.30; found: 1949.31 [M+Na]$^+$.

Preparation of BTM-NMs and BTG-NMs

BTM (5 mg) was dissolved in DMF (5 mL) and used as a stock solution. Then, 0.6 mL of the stock solution was added dropwise into deionized water (1.4 mL) containing 0.1 vol% Tween 80 under vigorous stirring. An NM dispersion of the BTM-NMs in aqueous solution (0.4 mg/mL) was obtained after dialyzing (MW 3500) with water to remove excess Tween 80 and DMF. BTG-NMs were prepared using BTG (5 mg) according to the same steps as those described for BTM-NM formation. To determine the concentration of BTM in the NM suspension, water was first removed by lyophilization, and the solid sample of the NMs was dissolved in DMF. The amount of BTM in DMF was calibrated based on a standard curve of concentration *vs.* absorbance determined by UV-Vis spectroscopy.

Detection of singlet oxygen generation in water

ABDA was used to evaluate the $^1O_2$ generation of the BTM-NMs in water. In this method, ABDA was dissolved in water (3 mL, 0.01 μg mL^{-1}), and then a solution of BTM-NMs in water (20 μL, 0.5 mg mL^{-1}) was added. The resulting solution was then subjected to light irradiation from a 665 nm LED lamp with a light density of 20 mW cm^{-2} that was set near (approximately 2 cm) to the quartz cuvette. At each predetermined

Accepted Manuscript

This article is protected by copyright. All rights reserved.

interval, the absorption spectrum of the solution was recorded. ABDA in water (3 mL, 0.01 μg mL^{-1}) was used as a control.

Cell culture

MDA-MB-231 (breast cancer) cells and MCF-10A (breast normal) cells were cultured in DMEM containing 10% FBS, penicillin (100 U mL^{-1}), and streptomycin (100 μg mL^{-1}) in a humidified atmosphere with 5% CO_2 at 37 °C.

Cell uptake of BTM-NMs

MDA-MB-231 cells were seeded in 35-mm plastic-bottomed Ibidi μ-dishes and allowed to grow for 24 h. After incubation with BTM-NMs (at a BTM dose of 8 μg mL^{-1}) in culture medium for 24 h, the cells were washed three times with PBS (pH 7.4) and then fixed with 4.0% formaldehyde at room temperature for 15 min. After being washed with PBS, the cells were stained with DAPI (1 μg mL^{-1}) for 15 min. After being washed again with PBS, the cells were observed under a confocal microscope (100 × oil objective, 408/561 nm excitation).

Localization of BTM-NMs

MDA-MB-231 cells or MCF-10A cells were seeded according to the abovementioned procedure. The cells were washed three times with PBS (pH 7.4) and then incubated with BTM-NMs (at a BTM dose of 8 μg mL^{-1}) in culture medium at 37 °C. After 24 h of incubation, the medium was removed, and the cells were washed three times with PBS and treated with LysoTracker Green DND-99 solution (50 nM) in DMEM at 37 °C for 30 min. After being washed with fresh medium, the cells were irradiated with or without an LED light (665 nm, 20 mW cm^{-2}) for 15 min. Finally, the cells were examined under an inverted Nikon confocal microscope (100 × oil objective, 488/561 nm excitation).

Phototoxicity assay

The cells were seeded into a 96-well plate at density of 1×10^4 cells per well within DMEM (100 μL) for 24 h. The culture medium was then replaced with fresh culture medium (100 μL) containing either BTM-NMs or BTG-NMs at different PS concentrations. After 24 h, the cells were washed three times with PBS, and the wells were refilled with 100 μL of fresh culture medium. The plates were irradiated with 665 nm LED light for 30 min. The distance between the 96-well plate and light source is approximately 2 cm, and the light power at the 96-well plate position is 20 mW cm^{-2}. The cells were further cultured for 12 h, and the culture medium from each well was replaced with 100 μL of medium containing MTT (0.5 mg mL^{-1}). After another 4 h of incubation, culture supernatants were removed, and DMSO (100 μL) was added into each well. The plate was gently shaken for 10 min, and the absorbance at 570 nm was recorded on a BioTek Synergy H4 microplate reader. The relative cell viability compared to the control wells treated with only medium was calculated using $[A]_{test}/[A]_{control}$, where $[A]_{test}$ and $[A]_{control}$ are the average absorbance of the test and control samples, respectively.

Statistical analysis

Statistical analysis was performed using Student's t-test. Data were collected from three or more replicates for each experiment and are presented as the mean ± standard deviation. Differences were considered to be statistically significant (*p<0.05, **p<0.01).

Acknowledgements

This work was financially supported by National Natural Science Foundation of China (51403081 and 21302072), Natural Science Foundation of Jiangsu Province (BK20140137), the Fundamental Research Funds for the Central Universities (JUSRP51629B), the Open Foundation of Key Laboratory of Carbohydrate Chemistry & Biotechnology Ministry of Education (KLCCB-KF201705), Max Planck Society International Partner Group Program, High-end Foreign Experts Recruitment Program, and The Thousand Talents Plan (Young Professionals).

Conflict of interest

The authors declare no conflict of interest.

Keywords: BODIPY• breast cancer • photodynamic therapy • photosensitizer • targeted delivery

[1] a) D. E. Dolmans, D. Fukumura, R. K. Jain, *Nat. Rev. Cancer* **2003**, *3*, 380-387; b) S. B. Brown, E. A. Brown, I. Walker, *Lancet Oncol.* **2004**, *5*, 497-508; c) A. P. Castano, P. Mroz, M. R. Hamblin, *Nat. Rev. Cancer* **2006**, *6*, 535-545; d) J. P. Celli, B. Q. Spring, I. Rizvi, C. L. Evans, K. S. Samkoe, S. Verma, B. W. Pogue, T. Hasan, *Chem. Rev.* **2010**, *110*, 2795-2838; e) J. M. Dabrowski, L. G. Arnaut, *Photochem. Photobiol. Sci.* **2015**, *14*, 1765-1780; f) Y. Shen, A. J. Shuhendler, D. Ye, J.-J. Xu, H.-Y. Chen, *Chem. Soc. Rev.* **2016**, *45*, 6725-6741.

[2] a) M. Ethirajan, Y. Chen, P. Joshi, R. K. Pandey, *Chem. Soc. Rev.* **2011**, *40*, 340-362; b) J. Zhao, W. Wu, J. Sun, S. Guo, *Chem. Soc. Rev.* **2013**, *42*, 5323-5351; c) J. Zhao, K. Xu, W. Yang, Z. Wang, F. Zhong, *Chem. Soc. Rev.* **2015**, *44*, 8904-8939; d) J. Zhou, J. Song, L. Nie, X. Chen, *Chem. Soc. Rev.* **2016**, *45*, 6597-6626.

[3] a) E. D. Sternberg, D. Dolphin, C. Bruckner, *Tetrahedron* **1998**, *54*, 4151-4202; b) S. K. Pushpan, S. Venkatraman, V. G. Anand, J. Sankar, D. Parmeswaran, S. Ganesan, T. K. Chandrashekar, *Curr. Med. Chem.: Anti-Cancer Agents* **2002**, *2*, 187-207; c) A. E. O'Connor, W. M. Gallagher, A. T. Byrne, *Photochem.Photobiol.***2009**, *85*, 1053-1074.

[4] a) M. Taniguchi, J. S. Lindsey, *Chem. Rev.* **2017**, *117*, 344-535; b) J. D. Spikes, *J. Photochem. Photobiol., B* **1990**, *6*, 259-274.

[5] a) R. Bonnett, *Chem. Soc. Rev.* **1995**, *24*, 19-33; b) L. M. Moreira, F. V. dos Santos, J. P. Lyon, M. Maftoum-Costa, C. Pacheco-Soares, N. S. da Silva, *Aust. J. Chem.* **2008**, *61*, 741-754.

[6] a) M.-R. Ke, S.-L. Yeung, D. K. P. Ng, W.-P. Fong, P.-C. Lo, *J. Med. Chem.* **2013**, *56*, 8475−8483; b) H. He, P.-C. Lo, S.-L. Yeung, W.-P. Fong, D. K. P. Ng, *Chem. Commun.* **2011**, *47*, 4748-4750; c) A. Kamkaew, S. H. Lim, H. B. Lee, L. V. Kiew, L. Y. Chung, K. Burgess, *Chem. Soc. Rev.* **2013**, *42*, 77-88.

[7] a) D. K. Chatterjee, L. S. Fong, Y. Zhang, *Adv. Drug Delivery Rev.* **2008**, *60*, 1627−1637; b) M. R. Detty, S. L. Gibson, S. J. Wagner, *J. Med. Chem.* **2004**, *47*, 3897-3915.

[8] a) A. S. Derycke, P. A. de Witte, *Adv. Drug Delivery Rev.* **2004**, *56*, 17-30; b) H.-I. Chang, M.-K. Yeh, *Int. J. Nanomed.* **2012**, *7*, 49-60.

[9] a) E. R. Gillies, J. M. J. Frechet, *Drug Discovery Today* **2005**, *10*, 35-43; b) W. Hu, H. Ma, B. Hou, H. Zhao, Y. Ji, R. Jiang, X. Hu, X. Lu, L. Zhang, Y. Tang, Q. Fan, W. Huang, *ACS Appl. Mater. Interfaces* **2016**, *8*, 12039-12047; (c) Y. Zhang, C. Teh, M. Li, C. Y. Ang, S. Y. Tan, Q. Qu, V. Korzh, Y. Zhao, *Chem. Mater.* **2016**, *28*, 7039-7050.

[10] a) C. J. F. Rijcken, O. Soga, W. E. Hennink, C. F. van Nostrum, *J. Controlled Release* **2007**, *120*, 131-148; b) J. Tian, L. Ding, H. Ju, Y.

Accepted Manuscript

This article is protected by copyright. All rights reserved.

Yang, X. Li, Z. Shen, Z. Zhu, J.-S. Yu, C. J. Yang, *Angew. Chem. Int. Ed.* **2014**, *53*, 9544-9549; *Angew. Chem.* **2014**, *126*, 9698-9703.

[11] a) L. Pan, J. Liu, J. Shi, *Adv. Funct. Mater.* **2014**, *24*, 7318-7327; b) K. Yang, L. Feng, X. Shi, Z. Liu, *Chem. Soc. Rev.* **2013**, *42*, 530-547; c) X. Ma, S. Sreejith, Y. Zhao, *ACS Appl. Mater. Interfaces* **2013**, *5*, 12860-12868; d) X. Ma, Q. Qu, Y. Zhao, *ACS Appl. Mater. Interfaces* **2015**, *7*, 10671-10676.

[12] a) D. K. Chatterjee, L. S. Fong, Y. Zhang, *Adv. Drug Delivery Rev.* **2008**, *60*, 1627-1637; b) S. S. Lucky, K. C. Soo, Y. Zhang, *Chem. Rev.* **2015**, *115*, 1990-2042.

[13] a) H. Koo, M. S. Huh, I.-C. Sun, S. H. Yuk, K. Choi, K. Kim, I. C. Kwon *Acc. Chem. Res.* **2011**, *44*, 1018−1028; b) S. Cui, D. Yin, Y. Chen, Y. Di, H. Chen, Y. Ma, S. Achilefu, Y. Gu, *ACS Nano* **2013**, *7*, 676-688; c) L. Huang, Z. Li, Y. Zhao, Y. Zhang, S. Wu, J. Zhao, G. Han, *J. Am. Chem. Soc.* **2016**, *138*, 14586-14591.

[14] a) X. Chen, L. Hui, D. A. Foster, C. M. Drain, *Biochemistry* **2004**, *43*, 10918-10929; b) S. Singh, A. Aggarwal, S. Thompson, J. o. P. C. Tomé, X. Zhu, D. Samaroo, M. Vinodu, R. Gao, C. M. Drain, *Bioconjugate Chem.* **2010**, *21*, 2136-2146; c) F. Hammerer, G. Garcia, S. Chen, F. Poyer, S. Achelle, C. Fiorini-Debuisschert, M.-P. Teulade-Fichou, P. Maillard, *J. Org. Chem.* **2014**, *79*, 1406-1417.

[15] I. Laville, S. Pigaglio, J.-C. Blais, F. Doz, B. Loock, P. Maillard, D. S. Grierson, J. Blais, *J. Med. Chem.* **2006**, *49*, 2558-2567.

[16] a) J. H. Ahire, I. Chambrier, A. Mueller, Y. Bao, Y. Chao, *ACS Appl. Mater. Interfaces* **2013**, *5*, 7384–7391; b) L. Yin, Y. Chen, Z. Zhang, Q. Yin, N. Zheng, J. Cheng, *Macromol. Rapid Commun.* **2015**, *36*, 483−489.

[17] a) D. Brevet, M. Gary-Bobo, L. Raehm, S. Richeter, O. Hocine, K. Amro, B. Loock, P. Couleaud, C. Frochot, A. Morere, P. Maillard, M. Garcia, J. O. Durand, *Chem. Commun.* **2009**, 1475–1477; b) M. Gary-Bobo, Y. Mir, C. Rouxel, D. Brevet, I. Basile, M. Maynadier, O. Vaillant, O. Mongin, M. Blanchard-Desce, A. Morere, M. Garcia, J. O. Durand, L. Raehm, *Angew. Chem. Int. Ed.* **2011**, *50*, 11425 – 11429; *Angew. Chem.* **2011**, *123*, 11627–11631.

[18] a) M. Delbianco, P. Bharate, S. Varela-Aramburu, P. H. Seeberger, *Chem. Rev.* **2016**, *116*, 1693–1752; b) Z. Ye, Q. Zhang, S. Wang, P. Bharate, S. Varela-Aramburu, M. Lu, P. H. Seeberger, J. Yin, *Chem. Eur. J.* **2016**, *22*, 15216-15221; c) Q. Zhang, Y. Cai, X.-J. Wang, J.-L. Xu, Z. Ye, S. Wang, P. H. Seeberger, J. Yin, *ACS Appl. Mater. Interfaces* **2016**, *8*, 33405-33411.

[19] J. M. Poolman, C. Maity, J. Boekhoven, L. van der Mee, V. A. A. le Sage, G. J. M. Groenewold, S. I. van Kasteren, F. Versluis, J. H. van Esch, R. Eelkema, *J. Mater. Chem. B* **2016**, *4*, 852-858.

[20] X.-J. Jiang, S.-L. Yeung, P.-C. Lo, W.-P. Fong, D. K. P. Ng, *J. Med. Chem.* **2011**, *54*, 320-330.

[21] H. Lu, N. Kobayashi, *Chem. Rev.* **2016**, *116*, 6184-6261.

[22] N. M. Idris, M. K. Gnanasammandhan, J. Zhang, P. C. Ho, R. Mahendran, Y. Zhang, *Nat. Med.* **2012**, *18*, 1580-1585.

[23] X. Wang, H. Fang, Z. Huang, W. Shang, T. Hou, A. Cheng, H. Cheng, *J. Mol. Med.* **2013**, *91*, 917−927.

[24] J. Hu, Y. Tang, A. H. Elmenoufy, H. Xu, Z. Cheng, X. Yang, *Small* **2015**, *11*, 5860-5887.

[25] Q. Zhang, X. Wang, P.-Z. Li, K. T. Nguyen, X.-J. Wang, Z. Luo, H. Zhang, N. S. Tan, Y. Zhao, *Adv. Funct. Mater.* **2014**, *24*, 2450−2461.

[26] S. H. Kim, J. E. Lee, S. M. Sharker, J. H. Jeong, I. In, S. Y. Park, *Biomacromolecules* **2015**, *16*, 3519−3529.

[27] (a) Q. Zhang, K. G. Neoh, L. Xu, S. Lu, E. T. Kang, R. Mahendran, E. Chiong, *Langmuir* **2014**, *30*, 6151−6161; (b) H.-J. Xiang, H. P. Tham, M. D. Nguyen, S. Z. F. Phua, W. Q. Lim, J.-G. Liu, Y. Zhao, *Chem. Commun.* **2017**, *53*, 5220-5223.

WILEY-VCH
Accepted Manuscript

This article is protected by copyright. All rights reserved.

10.1002/chem.201702935

Table of Contents

FULL PAPER

Breast cancer cells recognize and internalize nanomicelles co-assembled from a mannose-conjugated BODIPY photosensitizer and Tween 80. These nanomicelles exhibit excellent targeted delivery of the photosensitizer that not only leads to selective cancer cell death but also minimizes damage to normal cells after 665-nm LED light irradiation.

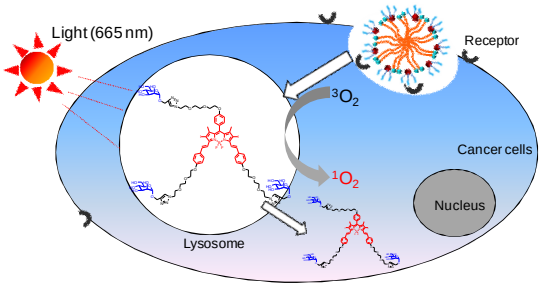

Quan Zhang, Ying Cai, Qiu-Yan Li, Lin-Na Hao, Zheng Ma, Xiao-Jun Wang, Jian Yin**

Targeted Delivery of Mannose-Conjugated BODIPY Photosensitizer by Nanomicelles for Photodynamic Breast Cancer Therapy

Accepted Manuscript

This article is protected by copyright. All rights reserved.